RESEARCH ARTICLE SUMMARY

CHROMATIN

Distortion of histone octamer core promotes nucleosome mobilization by a chromatin remodeler

Kalyan K. Sinha, John D. Gross,* Geeta J. Narlikar*

INTRODUCTION: The establishment of specific gene expression states during the course of development, as well as their maintenance through the disruptive events of transcription, DNA replication, and DNA repair, requires rapid rearrangements of chromatin structure. Adenosine 5′-triphosphate (ATP)–dependent chromatin remodeling motors are the workhorses that enable dynamic changes in chromatin structure. These motors have the formidable task of mobilizing DNA in the context of a nucleosome, which contains ~150 base pairs of DNA tightly wrapped around an octamer of histone proteins. Yet, compared to other essential motors such as myosins and helicases, little is known about the biochemical mechanisms of chromatin remodeling motors, limiting an understanding of how their functions are regulated.

RATIONALE: Two classes of chromatin remodeling motors, the ISWI class and the SWI-SNF class, have proved to be powerful model systems for asking mechanistic questions. Notably, both the ISWI and SWI-SNF family motors can move DNA without disassembling the histone octamer. Further, recent studies indicate that ISWI family motors translocate DNA out of the nucleosome before feeding DNA into the nucleosome, a result that is difficult to reconcile with rigid Lego-block–like models of the histone octamer. One way the seemingly complex task of chromatin remodeling may be facilitated is by distorting the histone octamer. Here, we probe this possibility by carrying out methyl transverse relaxation–optimized nuclear magnetic resonance (methyl-TROSY NMR) experiments on the ~450-kilodalton complex of a nucleosome with an activated form of the major ISWI family remodeling motor from humans, SNF2h. Methyl-TROSY is a powerful tool capable of providing site-specific information on the dynamics of individual amino acid residues. We have further tested the functional relevance of information obtained from these NMR experiments in the context of chromatin remodeling reactions by introducing site-specific cysteine cross-links at the histone H3-H4 interface. These cross-links have provided a means to restrain backbone movements and thus, have allowed us to test the importance of octamer deformability during ATP-dependent remodeling reactions.

RESULTS: We show that the dynamics of buried isoleucine, leucine, and valine residues in histone H4 change when the nucleosome is bound to SNF2h in the presence of the non-hydrolyzable ATP analog ADP-BeFx. NMR studies following the isoleucine residues of histone H2A further indicate that the changes induced upon SNF2h binding extend across the nucleosome. These results indicate that the histone octamer is deformed in the presence of SNF2h. Using site-specific disulfide bridges at the H3-H4 interface, we show that interfering with octamer deformation can inhibit nucleosome sliding by SNF2h or alter the directionality of nucleosome sliding. We further show that different classes of remodeling enzymes respond differently to these disulfide restraints. Disulfide bridges that inhibit SNF2h-mediated sliding allow sliding by the INO80 complex and increase octamer eviction by the SWI-SNF family complex, RSC.

ON OUR WEBSITE

Read the full article at http://dx.doi.org/10.1126/science.aaa3761

CONCLUSION: The histone core of a nucleosome is more plastic than previously imagined, and octamer deformation can play different roles based on the type of chromatin remodeling complex. ■

The list of author affiliations is available in the full article online.
*Corresponding author. Email: jdgross@cgl.ucsf.edu (J.D.G.); geeta.narlikar@ucsf.edu (G.J.N.)
Cite this article as K. K. Sinha *et al.*, *Science* **355**, eaaa3761 (2017). DOI: 10.1126/science.aaa3761

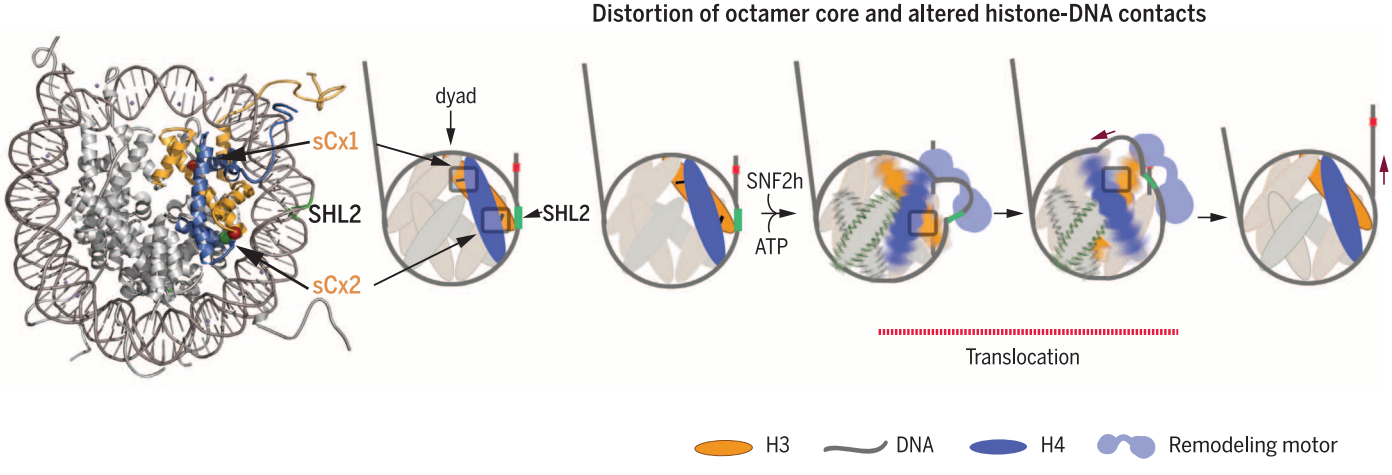

Model for role of octamer distortion in nucleosome sliding by SNF2h. Octamer deformation near SHL2 (inhibited by sCx2 cross-link) promotes initiation of DNA translocation, while deformation near the dyad (inhibited by sCx1 cross-link) helps accommodate strain caused by DNA translocation. These conformational changes allow for a net translocation of DNA from the exit site before any DNA is drawn in from the entry site.

RESEARCH ARTICLE

CHROMATIN

Distortion of histone octamer core promotes nucleosome mobilization by a chromatin remodeler

Kalyan K. Sinha,[1] John D. Gross,[2]* Geeta J. Narlikar[1]*

Adenosine 5′-triphosphate (ATP)–dependent chromatin remodeling enzymes play essential biological roles by mobilizing nucleosomal DNA. Yet, how DNA is mobilized despite the steric constraints placed by the histone octamer remains unknown. Using methyl transverse relaxation–optimized nuclear magnetic resonance spectroscopy on a 450-kilodalton complex, we show that the chromatin remodeler, SNF2h, distorts the histone octamer. Binding of SNF2h in an activated ATP state changes the dynamics of buried histone residues. Preventing octamer distortion by site-specific disulfide linkages inhibits nucleosome sliding by SNF2h while promoting octamer eviction by the SWI-SNF complex, RSC. Our findings indicate that the histone core of a nucleosome is more plastic than previously imagined and that octamer deformation plays different roles based on the type of chromatin remodeler. Octamer plasticity may contribute to chromatin regulation beyond ATP-dependent remodeling.

The establishment of specific gene expression states during the course of development as well as their maintenance through the disruptive events of transcription, DNA replication, and DNA repair requires rapid rearrangements of chromatin structure (*1*, *2*). Adenosine 5′-triphosphate (ATP)–dependent chromatin remodeling motors are the workhorses that enable dynamic changes in chromatin structure. Different families of chromatin remodeling motors have diverse biological roles ranging from gene activation to DNA repair (*2*, *3*). Yet, compared to other essential motors such as myosins and helicases, relatively little is known about the biochemical mechanisms of chromatin remodeling motors, limiting an understanding of how their functions are regulated.

Chromatin remodeling motors have the formidable task of mobilizing DNA in the context of a nucleosome, which contains ~150 base pairs (bp) of DNA tightly wrapped around an octamer of histone proteins (*4*). Two classes of chromatin remodeling motors, the ISWI class and the SWI-SNF class, have proved to be powerful model systems for asking mechanistic questions. Previous work has shown that motors from both these classes can translocate on naked DNA (*5*–*8*). However, it is not known how such translocation occurs in the context of the structural constraints placed by the histone octamer. Notably, both the ISWI and SWI-SNF family motors can move DNA without disassembling the histone octamer (*2*, *3*). It has been suggested that these motors can feed in DNA and propagate a DNA loop across the histone octamer (*2*). However, recent studies indicate that ISWI family motors translocate DNA out of the nucleosome before feeding DNA into the nucleosome, a result that is difficult to reconcile with the loop propagation model (*9*). It has also been proposed that chromatin remodelers may be able to drive a conformational change in the octamer itself (*10*–*16*). If such distortions can be demonstrated, this would provide a new class of models to explain remodeling mechanisms. Yet, it has been difficult to investigate the existence of conformational changes within the histone core largely owing to the limitations of available methods. For example, to date there are no high-resolution structures of a chromatin remodeling motor bound to a nucleosomal substrate.

Recent advances in high-resolution ^{1}H-^{13}C transverse relaxation–optimized nuclear magnetic resonance (methyl-TROSY NMR) spectroscopy provide an opportunity to directly investigate conformational changes within the histone octamer (*17*). Methyl-TROSY NMR is a powerful method that has been used to study dynamics at residue-level resolution in complexes as large as the ~670-kDa proteosome and the ~200 kDa nucleosome (*17*–*20*). Here, we report the results from applying this method to the ~450-kDa complex of a nucleosome with the major ISWI family remodeling motor from humans, SNF2h, bound to an activated state of ATP. We also report the results of biochemical experiments derived from the NMR data to test the functional roles of octamer distortion.

SNF2h alters the environment of buried histone residues in an activated ATP state

Our previous work has indicated that SNF2h functions most optimally as a dimer, with one protomer binding on either side of a nucleosome (*21*). Additionally, in the presence of the ATP analog ADP-BeFx, SNF2h engages the histone H4 tail, an allosteric activator of ISWI enzymes (*22*–*25*). This analog also promotes a restricted conformation of the adenosine triphosphatase (ATPase) active site (*26*). We therefore reasoned that NMR studies carried out in the presence of ADP-BeFx would mimic either an activated ground state or a transition state. We probed histone H4 in a nucleosome by methyl-TROSY NMR spectroscopy in the presence of ADP-BeFx. This method uses selective ^{13}C methyl group labeling of Ile, Leu, or Val (ILV) residues in an otherwise deuterated protein environment to exploit the line narrowing afforded by cross-correlated relaxation of CH dipolar couplings in a heteronuclear multiple quantum coherence experiment (*17*, *27*). The assembled nucleosomes contain ILV-labeled histone H4 and fully deuterated H3, H2A, and H2B. The methyl-TROSY spectrum of ILV-labeled H4 is well resolved, and a high degree of overlap was observed between the published spectra of *Drosophila* nucleosomes and our spectrum, as observed by the small Δδ (parts per million, ppm) values (fig. S2) (*20*). It was therefore possible to assign all the cross-peaks based on the previously published spectra of *Drosophila* nucleosomes (*20*) (Fig. 1A and figs. S1 and S2).

Numerous cross-peaks were perturbed upon addition of saturating concentrations of SNF2h to the nucleosome. These perturbations included reductions in resonance intensities and/or changes in chemical shift, as well as the appearance of new cross-peaks. The new cross-peaks can in principle arise from the natural abundance of ^{13}C in the unlabeled SNF2h. An NMR spectrum of unlabeled SNF2h bound to unlabeled nucleosomes did not show any cross-peaks that overlap with these new cross-peaks (fig. S3). This result is consistent with the new cross-peaks in Fig. 1 arising from the ILV-labeled H4 instead of SNF2h. Yet, to be conservative, we only investigate the origins for the reduction in resonance intensities of the ILV cross-peaks in H4. In this context, we first tested if the observed perturbations arise from disassembly of nucleosomes by comparing the NMR spectra of free histone ILV-labeled H4 with that of the SNF2h-nucleosome complex (fig. S4). We found no substantial overlap in cross-peaks, indicating that the observed NMR changes in the SNF2h-nucleosome complex spectrum are not due to dissociation of histone H4. Dynamic light-scattering experiments carried out under NMR conditions also confirmed a largely homogeneous SNF2h-nucleosome complex (fig. S5).

Given the above controls, we interpret the reductions in resonance intensities as reflecting a change in the magnetic environment of the H4 residues within an intact nucleosome. Such resonance broadening results from an increase in dephasing of transverse magnetization. This could be a manifestation of (i) an increase in molecular weight, (ii) exchange between bound and unbound states of the nucleosome, (iii) proximity of histone residues to nondeuterated SNF2h, or (iv) induction of protein dynamics

[1]Department of Biochemistry and Biophysics, University of California San Francisco, San Francisco, CA 94158, USA. [2]Department of Pharmaceutical Chemistry, University of California San Francisco, San Francisco, CA 94158, USA. *Corresponding author. Email: jdgross@cgl.ucsf.edu (J.D.G.); geeta.narlikar@ucsf.edu (G.J.N.)

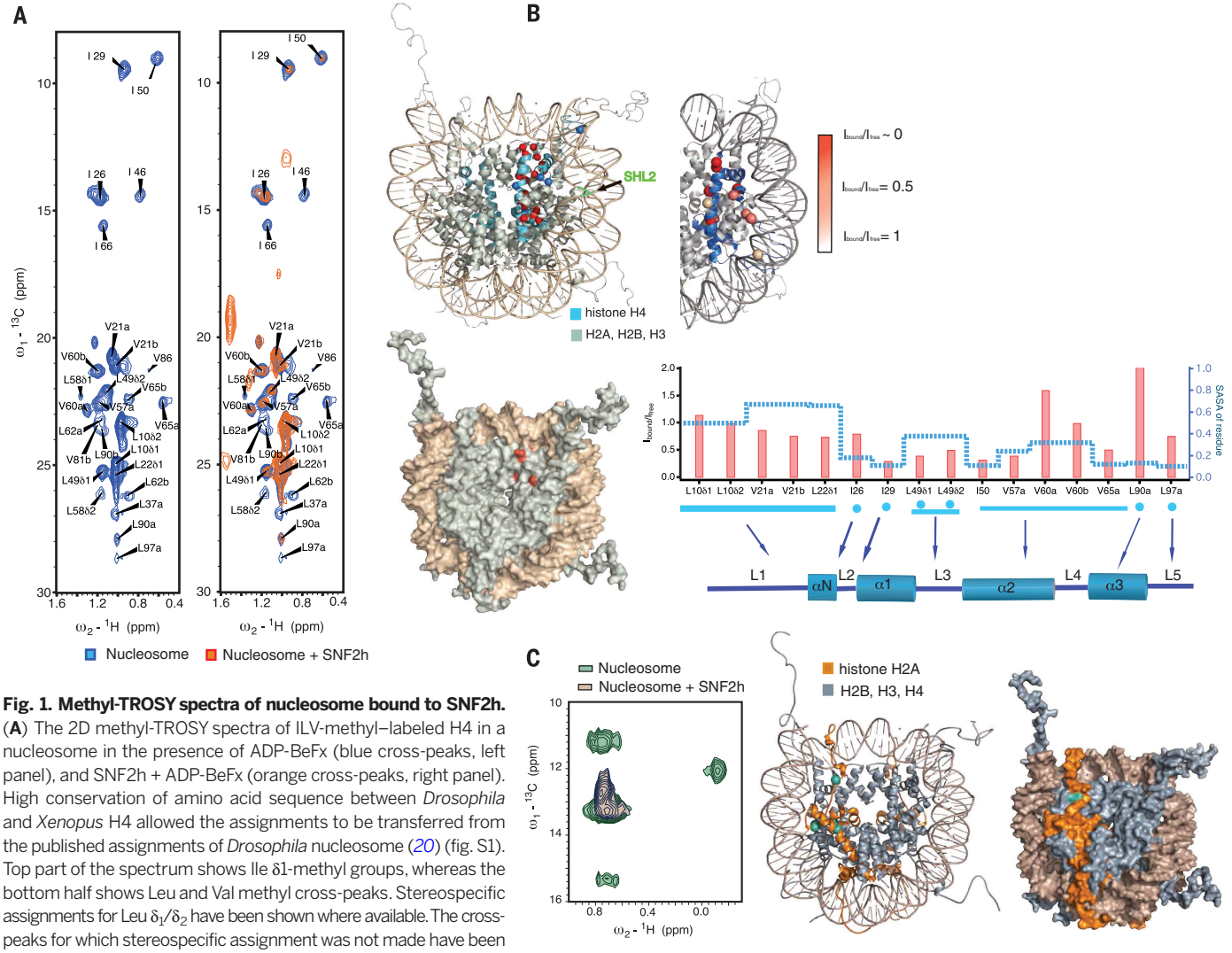

Fig. 1. Methyl-TROSY spectra of nucleosome bound to SNF2h. (**A**) The 2D methyl-TROSY spectra of ILV-methyl–labeled H4 in a nucleosome in the presence of ADP-BeFx (blue cross-peaks, left panel), and SNF2h + ADP-BeFx (orange cross-peaks, right panel). High conservation of amino acid sequence between *Drosophila* and *Xenopus* H4 allowed the assignments to be transferred from the published assignments of *Drosophila* nucleosome (*20*) (fig. S1). Top part of the spectrum shows Ile δ1-methyl groups, whereas the bottom half shows Leu and Val methyl cross-peaks. Stereospecific assignments for Leu δ_1/δ_2 have been shown where available. The cross-peaks for which stereospecific assignment was not made have been arbitrarily assigned as "a" or "b". Cross-peaks that show small changes (e.g., L10, V21, V60) and cross-peaks that show decreased intensity due to resonance broadening (e.g., I50, L58, V57) can be seen in the spectrum of the complex. Nucleosome structure in the right panel (*67*) shows the location of the Cα of all the ILV residues in H4 (light blue); dark blue spheres: residues that do not change much upon binding of SNF2h; red spheres: residues that get broadened upon SNF2h binding (based on 1B). A surface representation of nucleosome structure shows how most of the ILVs (red) in H4 (blue) are buried. The location of the superhelix location 2 (SHL2) is shown in green on the DNA. (**B**) Quantification of cross-peak broadening for H4 residues where cross-peaks in the bound state have not disappeared. Left panel: distribution of ILV residues showing peak broadening depicted on nucleosome structure. The intensity of red color represents extent of broadening. Residues shown as deep red spheres disappear completely, and hence, are broadened to a greater extent. Right panel: red bars (left *y* axis) represent relative peak volumes of residues in the nucleosome-SNF2h complex (I_{bound}) compared to those in the nucleosome alone (I_{free}) for residues that give observable signals in both spectra. The two sets of spectra were normalized using the volumes of their respective L10δ2 peak, which does not show broadening upon SNF2h binding. The blue dashed line (right *y* axis) shows solvent-accessible surface area (SASA) of the corresponding ILV residues. SASA was calculated from the PDB structure file 1kx5 using the program POPS (*68*). The SASA values are for the entire residue and represent fraction of exposed surface area. The location of different ILV residues in H4 can be read from the cartoon below showing the H4 polypeptide chain with its structural elements (loops L1 to L5, helices αN to α3) (*67*). (**C**) The 2D methyl-TROSY spectra of Ile-methyl–labeled H2A within a nucleosome showing the Ile region of the spectrum. The spectrum of the SNF2h-bound form of the nucleosome (brown) with ADP-BeFx shows peak broadening, as well as the appearance of a new peak, when overlaid on the spectrum of nucleosome alone with ADP-BeFx (green). The two versions of nucleosome structures on the right show H2A in orange, and the Ile residues in H2A as green spheres.

on a millisecond-microsecond (ms-μs) time scale in the vicinity of the labeled residues (*28*, *29*). Below, we investigate these possibilities.

An increase in molecular mass is expected to show largely uniform broadening of all the H4 residues. However, a quantification of the relative resonance broadening associated with the H4 residues showed that the residues that were broadened were not uniformly distributed (Fig. 1B). Some residues buried in the core of the nucleosome are only marginally affected by addition of SNF2h [e.g., Ile^{26} (I26), Val^{60} (V60), and Leu^{90} (L90)], whereas other residues are substantially affected (e.g., Ile^{29}, Ile^{50}, and Val^{65}). These results suggest that an increase in mass is not the sole source of resonance broadening.

The dissociation constant (K_d) of SNF2h for binding nucleosomes under these conditions is ~150 nM (fig. S6). Given a range of diffusion-limited binding rates (10^4 to 10^6 M^{-1} s^{-1}) (*30*) for protein-protein interactions, the dissociation rate constants are slow (<0.15 s^{-1}) relative to the NMR chemical-shift time scale, suggesting that the broadening does not arise from exchange between the bound and unbound states of the nucleosome.

Substantial previous work has suggested that ISWI enzymes bind near the superhelical location

2 (SHL2) on the nucleosome (Fig. 1A) (*31*–*33*). It is therefore possible that H4 ILV residues proximal to SHL2 are broadened by direct contacts with protonated SNF2h. Consistent with this possibility, Ile^{29}, which is closest to SHL2 (fig. S7; ~10.6 Å from the phosphate group of dT17 in SHL2), is substantially broadened. However, residues L49, I50, and V57, which are much further away (>20 Å from phosphate group of dT17 in SHL2) and substantially buried, also show a comparable extent of broadening (Fig. 1B). Direct contact between SNF2h and these residues would not be possible in a canonical nucleosome structure. We therefore interpret the data to suggest that either (i) binding of SNF2h on the exterior allosterically induces protein dynamics on a ms-μs time scale in buried regions of the octamer; or (ii) SNF2h opens up the octamer to directly contact residues that are normally buried. In either interpretation, the octamer would have to undergo a structural change that results in a change in the environment of buried histone residues.

To test if the SNF2h-induced changes are confined to a defined interface between histones H4 and H3 or affect a broader region of the nucleosome, we examined changes in H2A residues by NMR.

Unlike for H4, it was not possible to transfer the assignments for H2A ILV cross-peaks from previously published spectra of *Drosophila* nucleosomes to *Xenopus* nucleosomes, because of low sequence homology between *Xenopus* and *Drosophila* H2A (fig. S1). Isoleucine residue cross-peaks are well separated from the rather crowded spectral region of leucine and valine resonances (*34*). Accordingly, we focused on the Ile region of the *Xenopus* H2A spectrum, which has well-resolved cross-peaks (Fig. 1C, left panel). As with H4, broadening and chemical-shift changes are observed for resonances of H2A in the Ile region of the spectrum upon binding of SNF2h. Although we have not assigned the H2A cross-peaks, the Ile residues in H2A are mostly buried, suggesting that the effect of SNF2h on the histone core is not confined to H4 residues (Fig. 1C, right panel). H2A makes minimal contacts with the H3-H4 tetramer in the nucleosome structure (*4*). Therefore, the effect of SNF2h is either relayed to it via H2B or, possibly, SNF2h also makes direct contacts with H2A.

We next tested the functional consequences of altering histone regions that show perturbed resonances within the solvent-inaccessible octamer core, as well as near the histone-DNA interface.

Destabilizing DNA-histone contacts modestly enhances remodeling by SNF2h

The cross peak for the H4-I46 terminal methyl group is broadened in the SNF2h-nucleosome complex. This residue is proximal to H4-R45 (Arg^{45}), which makes contacts with nucleosomal DNA and is a SIN mutant location (*4*, *35*). These mutations were found in budding yeast as suppressors of defects in the SWI-SNF family of motors (*35*). The side chain of R45 inserts into the DNA minor groove and is thought to participate in the stability of histone-DNA interactions (*4*). Indeed, mutating R45 has been shown to increase thermally driven nucleosome mobilization (*36*, *37*). This raised the possibility that SNF2h mobilizes nucleosomes in part by destabilizing the interaction between H4-R45 and nucleosomal DNA, thereby resulting in altered dynamics of H4-I46. To test this possibility, we measured the effect of an H4-R45A (Arg^{45}→Ala) mutation on nucleosome remodeling by SNF2h. SNF2h moves nucleosomes positioned on one end of a short piece of DNA toward the center. We used a native gel-based assay that allows detection of such movement of nucleosomes. The rate constant for centering the mutant nucleosome was about twice as fast as for the wild-type (WT) nucleosome (fig. S7B). The small magnitude of the effect with SNF2h is similar to that of previous observations with the SWI-SNF family of chromatin remodeling enzymes (*37*, *38*). The twofold faster rate constant could reflect twofold faster remodeling by SNF2h or faster nonenzymatic reequilibration of the centered R45A nucleosomes back to the end position. Both possibilities imply that the interaction between R45 and DNA represents a relatively modest barrier for remodeling.

Restricting internal histone movements inhibits nucleosome sliding by SNF2h

We next investigated the functional relevance of the resonance perturbations observed in the

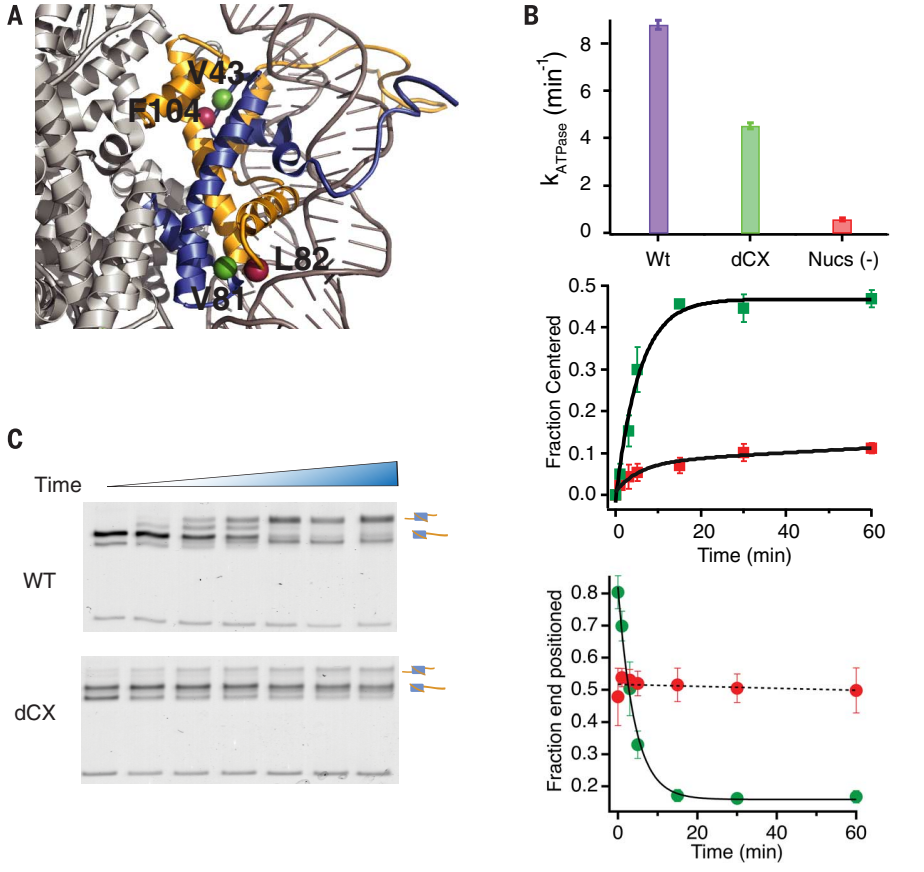

Fig. 2. Functional impact of restricting H3-H4 interface on SNF2h. (**A**) Location of residues mutated to cysteines. Residues L82 and F104 in H3, and V43 and V81 in H4, were mutated to Cys. (**B**) Comparison of SNF2h ATPase rates in the presence of WT (purple), dCX (green), and no nucleosomes (red). Error bars represent the SDs from three independent experiments. (**C**) Comparison of remodeling of WT and dCX nucleosomes by SNF2h. Left panels: representative gel for remodeling kinetics for WT (top panel) and dCX (bottom panel), respectively. Right panels: Quantification of the fraction of centered nucleosomes (top panel) and the fraction of end-positioned nucleosomes (bottom panel) as a function of time. WT data are in green and dCX data are in red. Time points (in minutes): 0, 1, 3, 5, 10, 20, and 60. Error bars are the SDs from three independent experiments. In the top right panel, the observed rate constant, k_{obs}, for the WT is 0.18 ± 0.03 min^{-1}. The rate constant for the minor fast phase of dCX (k_{1fixed}) was fixed to be the same as the k_{obs} for the WT. The rate constant for the major slow phase (k_{2obs}) with the constraint of k_{1fixed} = 0.18 min^{-1} was calculated to be 0.003 ± 0.001 min^{-1}. Fitting the entire time course for dCX to a single exponential gives a value of k_{obs}= 0.01 ± 0.001 min^{-1}. For all experiments with cysteine cross-linked nucleosomes, Cy3-labeled 601+60 DNA was externally added to the WT nucleosome samples to make the reaction conditions between the WT and cross-linked nucleosomes comparable to those of the cross-linked nucleosomes with some free DNA. The free DNA inhibits rates of remodeling in a dose-dependent manner (see supplementary methods for details).

octamer core. We reasoned that if we could restrict the flexibility of a large region of the buried H3-H4 interface, we could test if and how such restriction affects nucleosome sliding. Accordingly, using the crystal structure as a guide [Protein Data Bank (PDB) code: 1kx5], we introduced cysteine mutations that would lock the H3-H4 interface at two different locations by means of disulfide bridges (Fig. 2A): H3F104C-H4V43C (F104C: Phe^{104}→Cys; V43C: Val^{43}→Cys) and H3L82C-H4V81C (L82C: Leu^{82}→Cys; V81C: Val^{81}→Cys). The mutation V43C in H4 is proximal to residues Ile^{46} and Leu^{37}, for which the cross-peaks disappeared in the presence of SNF2h. Likewise, the cross-peak for V81C in H4 also disappeared in the presence of SNF2h. We chose the cysteine pairs such that the two side chains in H3 and H4 were oriented toward each other away from solvent, and were at most 5 Å apart in the structure. Because of this design, the disulfide bonds formed efficiently within a preassembled histone octamer in the presence of ambient oxygen upon removal of reducing agent (fig. S8A). Our design allowed formation of a largely uniform population of nucleosomes with dual disulfide-linked H3-H4 (referred to as dCX, Fig. 2B).

We first tested the ability of dCX nucleosomes to stimulate ATP hydrolysis by SNF2h because nucleosome-stimulated ATP hydrolysis is a defining feature of ISWI enzymes (*39*–*42*). We found that dCX nucleosomes also stimulated ATP hydrolysis, although slightly less (<twofold) than wild-type nucleosomes (Fig. 2B). This result suggested that SNF2h can bind to and recognize dCX nucleosomes.

Next, we investigated the effect of restricting octamer flexibility on nucleosome sliding using the native gel-based assay. We used single-turnover conditions with excess and saturating concentrations of SNF2h over nucleosomes to measure maximal rate constants. We found that in contrast to the small effects seen on ATP hydrolysis, sliding of the vast majority of dCX nucleosomes (>90%) by SNF2h was severely inhibited (Fig. 2C, ~60-fold inhibition). A small population (<10%) of the dCX nucleosomes appeared to be centered with rates comparable to those of wild-type nucleosomes. This population is consistent with the small population of uncross-linked histones (fig. S8A). To control for the effects of introducing the cysteine mutations, we measured the ability of SNF2h to remodel nucleosomes containing the cysteine mutants assembled under reducing conditions (dCH nucleosomes). SNF2h remodeled these nucleosomes with an efficiency similar to that of WT nucleosomes (fig. S8B). Together, these results suggest that the observed inhibition of nucleosome sliding is due to the disulfide cross-links.

Of the two cross-links, H3L82C-H4V81C, which we term sCX2, is in the vicinity of SHL2, the DNA region where the ATPase domain of SNF2h is proposed to bind, while the other cross-link, H3F104C-H4V43C, which we term sCX1, is closer to the vicinity of the dyad. We wondered if restricting the nucleosome with each of these cross-links separately would have similar or different effects compared to restricting the nucleosome with two cross-links simultaneously as in dCX. We therefore compared the effects of each cross-link individually. The sCX2 cross-link, markedly inhibits nucleosome sliding, similar to effects observed with the dCX nucleosomes (Fig. 3A). At first glance, the sCX1 cross-link also appears to inhibit nucleosome sliding, as seen by the reduction in the amount of centered nucleosomes. However, closer inspection of the data reveal some interesting differences. In contrast to sCX2, the sCX1 cross-link does not significantly inhibit nucleosome sliding away from the end position [compare WT versus sCX2 in Fig. 3A, right-most panel, to WT versus sCX1 (~fourfold inhibition) in Fig. 3B, right-most panel]. Instead, sCX1 reduces the fraction of centered nucleosomes because its remodeling leads to a greater proportion of alternative products (Fig. 3B, products denoted by the asterisk) that migrate faster than the end-positioned starting material on a native gel.

In vivo, SNF2h is found in larger complexes. A key SNF2h-containing complex is ACF, which consists of the subunit Acf1 in addition to SNF2h (*15*). The Acf1 subunit has been shown to extend the ability of SNF2h to sense flanking DNA length

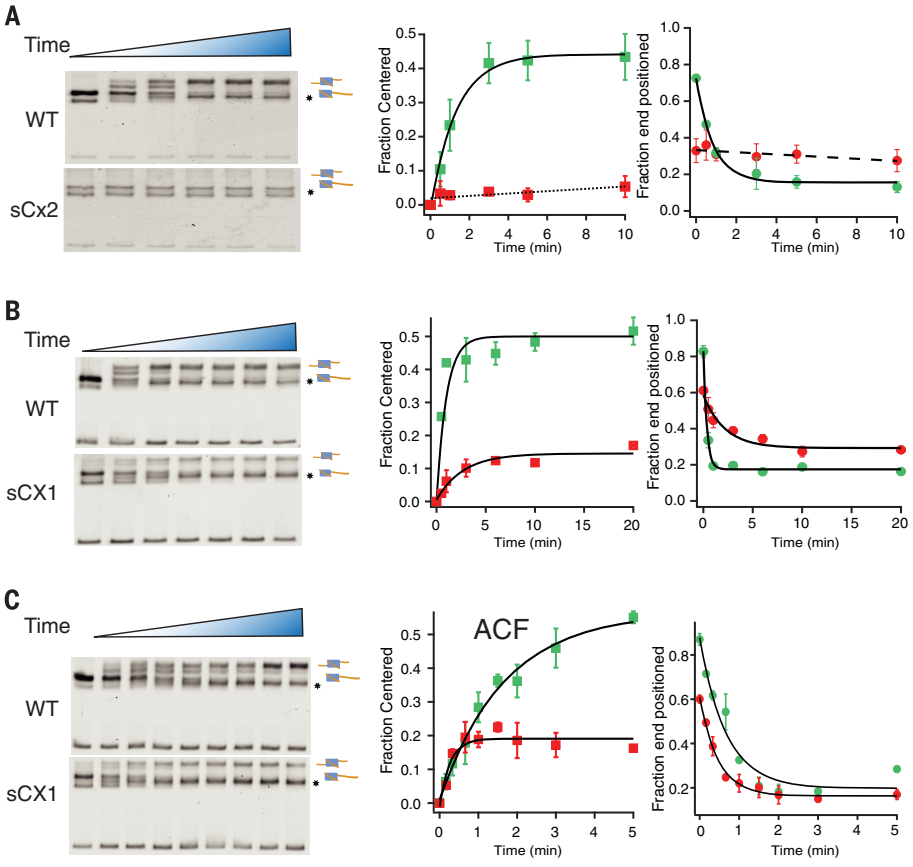

Fig. 3. Investigating the extent of H3-H4 flexibility required for remodeling by SNF2h and ACF. (**A**) Comparison of remodeling of WT and sCX2 nucleosomes by SNF2h and quantification of the fraction of centered nucleosomes (middle panel) and fraction of end-positioned nucleosomes (right panel) as a function of time. For the middle panel, WT: k_{obs} = 0.9 ± 0.1 min^{-1}; and sCX2: Because of the absence of clearly detectable product, a straight line has been drawn through the data points obtained from quantifying the signal at the locations where the centered nucleosomes migrate on the gel. Error bars are the SD from three independent repetitions of the experiment. (**B**) Comparison of remodeling of WT and sCX1 nucleosomes by SNF2h and quantification of the fraction of centered nucleosomes (middle panel) and fraction of end-positioned nucleosomes (right panel) as a function of time. For the middle panel (fraction centered), WT: k_{obs} = 1.5 ± 0.02 min^{-1}; sCx1: k_{obs} = 0.2 ± 0.05 min^{-1}. For the right panel (fraction end-positioned), WT: k_{obs} = 3 ± 0.6 min^{-1}; sCx1: k_{obs} = 0.7 ± 0.3 min^{-1}. Error bars are the average deviation from two independent repetitions of the experiment. (**C**) Comparison of remodeling of WT and sCX1 nucleosomes by ACF and quantification of the fraction of centered nucleosomes (middle panel) and fraction of end-positioned nucleosomes (right panel) as a function of time. For the middle panel (fraction centered), WT: k_{obs} = 0.64 ± 0.11 min^{-1}; sCx1: k_{obs} = 3.6 ± 1 min^{-1}. For the right panel (fraction end-positioned), WT: k_{obs} = 1.5 ± 0.3 min^{-1}; sCx1: k_{obs} = 2.2 ± 0.1 min^{-1}. Error bars represent the average deviation from two independent experiments. In all panels, data for WT nucleosomes are in green and data for disulfide cross-linked nucleosomes are in red.

and increase its ability to space nucleosomes (*15*). It was therefore informative to test if the nucleosome-centering ability of ACF was also affected by the SCX1 cross-link. ACF generated a slightly higher proportion of centered sCX1 nucleosomes compared to SNF2h. However, compared to its action on WT nucleosomes, ACF generated a much smaller fraction of centered sCX1 nucleosomes and a much larger fraction of alternative products (Fig. 3C, products denoted by the asterisk). These results suggest that octamer distortion proximal to the H3F104 and H4V43 residues is required for both SNF2h and ACF to effectively center nucleosomes.

To test if constraining octamer conformation inhibits nucleosome sliding by another class of remodeling enzymes, we investigated how the yeast INO80 complex acts on the doubly cross-linked dCX nucleosome. The INO80 remodeling complex is known to play important roles in double-strand break repair (*43*, *44*) and is thought to act by a mechanism that is distinct from that of the ISWI class of remodeling enzymes (*44*–*46*). INO80 activity was not inhibited on the dCX nucleosomes but instead showed a small (two-fold) rate enhancement compared to WT nucleosomes (Fig. 4A). That the dCX nucleosomes are remodeled comparable to WT by INO80 also indicates that the cross-links do not introduce major defects in nucleosome structure.

Restricting internal histone movements increases octamer eviction by yeast RSC complex

Previous work has shown that the SWI-SNF family of complexes and the ISWI family of complexes

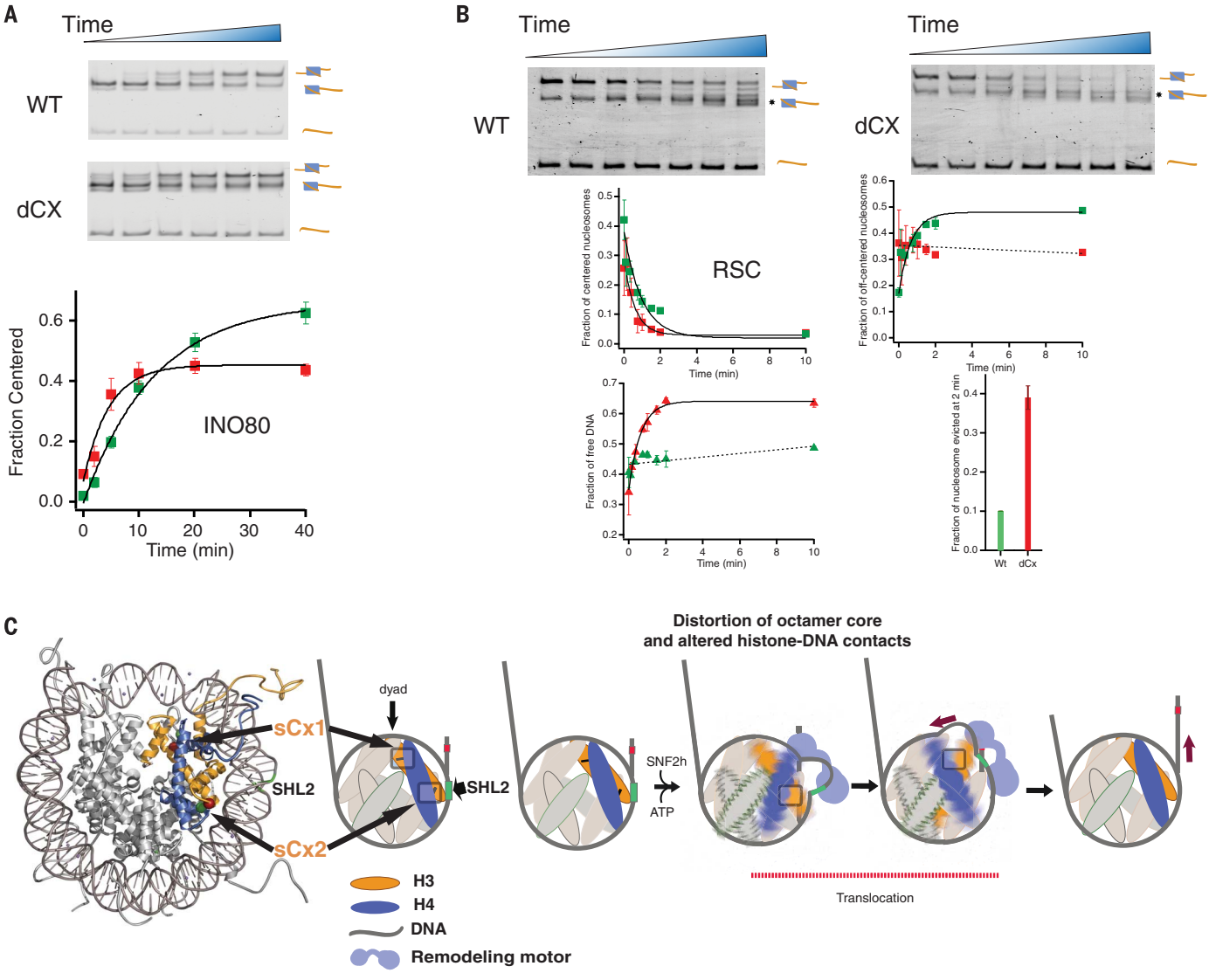

Fig. 4. Effects of constraining H3-H4 interface on additional remodeling complexes. (**A**) Comparison of remodeling rates of INO80 for WT (right panel: green squares, k_{obs}= 0.08 ± 0.006 min^{-1}) and dCX (right panel: red squares, k_{obs}= 0.22 ± 0.04 min^{-1}) nucleosomes. Left panels: representative gels for remodeling kinetics. Time points (in minutes): 0, 2, 5, 10, 20, and 40. Error bars represent the SDs from three independent experiments. (**B**) Comparison of RSC remodeling rates and outcomes for WT (green symbols) and dCX (red symbols) nucleosomes. For disappearance of centered nucleosomes, k_{WT} = 1.28 ± 0.02 min^{-1}, k_{dCX} = 1.8 ± 0.07 min^{-1}; For DNA eviction from dCX, k_{Evic} = 1.4 ± 0.2 min^{-1}; for appearance of end-positioned nucleosomes in WT, $k_{Off\text{-}centered}$ = 1.18 ± 0.18 min^{-1}. Error bars represent the average deviation from two independent experiments. The nucleosomal band that migrates faster than the end–positioned nucleosome is consistent with a product in which the octamer has moved beyond the DNA end as seen previously (*47*). (**C**) Model for role of octamer distortion in DNA mobilization by SNF2h. Histone octamer deformation proximal to SHL2 is coupled to translocation from SHL2 while deformation proximal to the dyad enables movement may allow the nucleosome to accommodate less DNA, thereby preventing the accumulation of any strain in the structure. These coupled conformational changes lead to a net translation of DNA from the exit site before any DNA is drawn in from the entry site. The location of the sCx1 and sCx2 cross-links is highlighted by the gray rectangles. The dashed lines in (B) are straight lines drawn through the data because the changes were too small to fit with an exponential.

differ in the types of remodeled products generated (*11*). For example, unlike most ISWI complexes, which move nucleosomes away from DNA ends, SWI-SNF complexes move nucleosomes toward DNA ends and sometimes beyond the DNA end (*47*). In addition, a small fraction of SWI-SNF products arise from eviction of the histone octamer, whereas ISWI complexes do not evict the histone octamer (*11*). The two types of complexes also differ in their sensitivity to DNA supercoiling and in the amounts of DNA translocated within a remodeling cycle: (*11*, *15*, *32*, *48*). These and other results have suggested that SWI-SNF and ISWI complexes use distinct mechanisms to mobilize nucleosomes. We therefore wondered if the SWI-SNF family of complexes would respond differently than the ISWI complex to constraining the H3-H4 interface. To test this possibility, we used RSC, the major SWI-SNF complex from budding yeast. We found that RSC slides both WT and dCX nucleosomes toward the DNA ends (Fig. 4B). However, a larger fraction of the centered dCX nucleosomes had their octamers evicted (Fig. 4B, bottom right panel; fraction of nucleosomes evicted at 2 min = ~0.4 compared to 0.1 for dCX versus WT nucleosomes, respectively). One implication of these results is that inhibiting octamer distortion biases the RSC products toward octamer eviction. It is also possible that these cross-links contribute to increased octamer eviction by reducing the stability of histone-DNA interactions, although such increased eviction is not observed with SNF2h and INO80.

Conclusions and implications

Our results suggest that the octamer core of a nucleosome is structurally plastic and that this plasticity can be exploited by chromatin remodeling motors to mobilize DNA within chromatin. Below we discuss the basis for this conclusion and the biological implications.

Here, we have leveraged the power of methyl-TROSY NMR to ask how a chromatin remodeling motor alters histone dynamics within the nucleosome at residue-level resolution. With this technique, we observed that binding of an activated form of SNF2h induced broadening of several cross-peaks corresponding to buried residues, consistent with a conformational change in the nucleosome core. Constraining the movement of buried histone residues in the vicinity of the DNA binding site of SNF2h strongly inhibited nucleosome sliding, but had modest effects on ATP hydrolysis. Together, these observations suggest that octamer deformation plays a major role in allowing SNF2h to use its intrinsic nucleosome-stimulated ATP hydrolysis activity to drive nucleosome sliding.

In the simplest model we can imagine, nucleosome-stimulated ATP hydrolysis generates an intermediate in which DNA deformation is thermodynamically coupled with octamer deformation. In such a model, deformation of DNA by SNF2h would stabilize deformation of the octamer and correspondingly, deformation of the octamer would promote deformation of DNA by SNF2h. The molecular basis for octamer deformation could then have two mutually compatible possibilities: (i) octamer deformation could arise indirectly as a result of changes propagated from remodeler-DNA interactions or; (ii) the octamer could be directly deformed by SNF2h. Indeed, previous cross-linking, foot-printing, and low-resolution electron miscroscopy studies suggest that ISWI enzymes make several contacts with the DNA and surface-exposed histone residues (*21*, *31*, *49*, *50*). It is also possible that SNF2h stabilizes a deformed octamer by making direct contacts with histone residues that are buried in the crystal structure.

The ATPase domain of ISWI enzymes has been mapped to bind near SHL2 (Fig. 4C), and this requires that ISWI enzymes like SNF2h translocate on DNA from a location where the DNA is tightly bound by histones (*31*). We find that constraining octamer flexibility in the vicinity of SHL2 via the H3L82C-H4V81C cross-link almost completely blocks nucleosome sliding by SNF2h. The simplest interpretation of this result suggests that initiation of DNA translocation from SHL2 relies on deforming the octamer proximal to this location. However, it remains formally possible that local alterations in nucleosome structure caused by the H3L82C-H4V81C cross-link inhibit some other aspect of SNF2h function before the actual sliding step, such as a conformational change in SNF2h that is required for translocation from SHL2. Our studies also help to rationalize more recent observations with ISWI enzymes that are difficult to explain on the basis of the canonical nucleosome structure. These studies, which were carried out with the yeast ISW2 complex, implied that ~7 bp of DNA is translocated from SHL2 toward the dyad and eventually out from the exit side before any DNA is translocated inward from the entry site (*9*) (Fig. 4C). Models using the canonical nucleosome structure require substantial stretching of the nucleosomal DNA, which is thought to impose a large strain on the nucleosome structure (*9*). We find that constraining octamer flexibility in the vicinity of the dyad via the H3F104C-H4V43C cross-link allows nucleosome sliding but substantially reduces the proportion of centered nucleosomes, generating instead a larger proportion of products that migrate faster on a native gel. This result suggests that the strain generated by translocation of DNA from SHL2 toward the dyad is alleviated by octamer deformation proximal to the dyad. In such a model, preventing octamer deformation near the dyad would lead to collapse of the partially remodeled nucleosomes to alternative positions on the DNA.

Our observations that the RSC and INO80 complexes respond differently than SNF2h to constraining octamer flexibility suggest that different remodeler families use the plasticity of the histone octamer in distinct ways. For INO80, it is not known where the ATPase subunit of the INO80 complex binds on a nucleosome (*46*). Therefore, it is possible that INO80 binds at a location where it is easier to break histone-DNA contacts, making its reaction less reliant on octamer deformation. The ATPase subunit of RSC, Sth1, has been suggested to bind near SHL2 in a manner analogous to the ISWI ATPase. However, unlike with SNF2h, the dCX double cross-links greatly increase octamer eviction. A recent RSC study has suggested that faster DNA translocation correlates with higher levels of octamer eviction, whereas slower translocation favors nucleosome sliding (*51*). Our results suggest that partitioning between sliding and eviction is further regulated by the distortability of the histone octamer. A distortable histone octamer may allow the DNA translocation activity of RSC to be accommodated in a manner that avoids octamer eviction. Overall, consistent with the previously observed mechanistic differences between SWI-SNF and ISWI [reviewed in (*15*)], our results suggest different roles for octamer distortion in the SWI-SNF and ISWI reactions.

Early work indicated that human SWI-SNF causes long-lived but reversible changes in the topology of nucleosomal arrays assembled on closed circular DNA templates (*52*, *53*). SWI-SNF action also generates mono- and dinucleosomes with altered nuclease accessibility that cannot be explained simply by nucleosome sliding or eviction (*10*, *12*, *13*). On the basis of the results obtained here, we propose that some of the stably altered nucleosome conformations implied by previous studies may involve an altered octamer conformation. Previous work has also shown that a disulfide cross-link between two H3 molecules at residue 110 does not inhibit remodeling by SWI-SNF; nor does general cross-linking of the histone octamer by dimethyl suberimidate (*54*, *55*). Although these previous studies did not directly investigate effects on octamer eviction, the published results are qualitatively consistent with our present results, suggesting that nucleosome sliding by RSC is still possible upon constraining octamer flexibility.

Most models for altering nucleosome structure are based on Lego block–like conceptions, where the individual histones can be removed or exchanged, but the octamer conformation is largely rigid. Indeed, in the absence of other protein factors, the canonical nucleosome conformation observed in crystal structures appears to be the most highly populated conformation in solution (*56*). At the same time, the possibility of alternative nucleosome conformations during nucleosome assembly and transcription has also been raised (*57*, *58*). Our results provide additional evidence that the octamer adopts more than one conformation and further demonstrate that octamer distortability is functionally relevant. Similar to the effects of SNF2h in the presence of ADP-BeFx, other stably bound chromatin regulators, specific histone modifications, and histone variants may also stabilize alternative octamer conformations. Indeed, several histone modifications are being discovered on core histone residues, raising the possibility that some of these alter the equilibrium between different octamer conformations within a nucleosome (*59*).

A distortable histone octamer may provide molecular explanations for how pioneer factors like FoxA and hormone receptors preferentially recognize DNA sequences buried within nucleosomes (*60*). In general, given the primary role of nucleosomes in regulating DNA accessibility, it is tempting to speculate that there are many nucleosome plasticity-based mechanisms exploited by the cell, which may be uncovered by future mechanistic studies.

Materials and methods

Protein expression, purification and isotope labeling

All the histones were expressed and purified from *E. coli* following published protocols (*61*) with some modifications for the isotopically labeled histones. For expression of deuterated histones, M9 minimal media was made in deuterium oxide (D_2O, Cambridge Isotope Ltd., CIL). The media contained 1,2,3,4,5,6,6-D7 Glucose (CIL or Sigma-Aldrich) as the energy source. For labeling the histones at ILV residues, $^{13}CH_3$-methyl group α-ketoisobutyrate and α-ketoisovalearate (CIL) were added to the M9 media as precursors (*62*). Deuteration and ILV labeling of the histones were confirmed by mass spectrometry. All the mutant versions of the histones were made by quick-change site-directed mutagenesis method. All the mutations were confirmed by sequencing the plasmids. N-terminally 6X-His tagged SNF2h was manually purified by cobalt affinity purification from an *Escherichia coli* Rosetta strain. After affinity purification, it was subjected to gel filtration on a Superdex 200 column, cation exchange through a SP5PW column, and anion exchange chromatography through a Q-HP column, in that order, to attain high purity.

Nucleosome assembly

Histone octamer was assembled from purified histones as described (*61*). The 601+20 (~167 bp) DNA fragment was made using restriction digestion of a plasmid carrying multiple copies of 601+20 DNA fragment as described previously (*61*). The 601+60 fragment was made by polymerase chain reaction as described previously (*21*). Nucleosomes were assembled using published gradient dialysis based protocols (*61*). The purification of the nucleosomes was carried out on a 10 to 30% glycerol gradient. A second purification was carried out on a Superdex-200 column before using the nucleosomes for NMR experiments.

Doubly cross-linked (dCx) and singly cross-linked (sCx1) nucleosomes were made using double Cys and single Cys variant histones H3 (L82CF104C for dCx; F104C for sCx1) and H4 (V43CV81C for dCx; V43C for sCx1). The histone variants were made by site-directed mutagenesis. The cysteine pairs were selected so as to have an interatomic distance ≤5 Å between the sulfur atoms facing each other (H3 F104C-H4 V43C distance was 5 Å and H3 L82C-H4 V81C distance was 4.8 Å). While selecting the residues for mutagenesis, it was ensured that the side chains point toward each other in the structure, to maximize the likelihood of disulfide bridge formation. The side chains of these residues were oriented away from solvent in the crystal structure. All the cysteine variant histone proteins were purified in the presence of excess dithiothreitol (DTT) during all the steps of protein purification. To purify the cysteine variants, only the gel filtration step was carried out. The subsequent ion-exchange step used for all the other histones was not carried out, because even small amounts of cyanate formed from urea (despite prior extensive deionization) in the ion-exchange buffer can reduce the fraction of available thiol groups for intermolecular disulfide bond formation between histones.

For dC octamer assembly, a variation of the standard protocol was followed so that any disulfide formation prior to the octamer assembly could be avoided. The assembly was carried out in the presence of 10 mM freshly made DTT in all the buffers. The column purification step too contained 5 mM DTT. After purification, the fractions containing the histone octamer were analyzed on a SDS gel. Most of the octamer formed (>90%) contained uncrosslinked H3 and H4, as expected. For dCX octamer formation, the dC octamer was subjected to oxidizing conditions. First, the dC octamer sample was diluted using the refolding buffer to a final octamer concentration of 5 μM to minimize the formation of any intermolecular cross-links. The diluted dC-octamer sample was dialyzed into octamer refolding buffer (pH 8.5) that did not contain any reducing agent. Three dialysis steps were carried out; the first two were overnight steps, and the third one was done for ~6 hours. The dialysis time can be increased in case the cross-linking is not complete. The cross-linking efficiency was confirmed by running the sample on a 15% SDS gel (fig. S8A and main text). Nucleosome assembly was carried out with the cross-linked octamers (dCX) as described previously except that none of the buffers used during the nucleosome assembly contained any reducing agent (*61*). The assembled nucleosomes were purified on a 10 to 30% glycerol gradient. The assembly of singly cross-linked (sCx1) nucleosomes was carried out by mixing tetramer of cross-linked H3-H4 with H2A-H2B dimer in the presence of Cy3 labeled 601 0-60 DNA.

NMR sample preparation and spectroscopy

The nucleosome storage buffer was exchanged with NMR buffer by dialysis. The NMR buffer was made in D_2O and contained 20 mM deuterated Tris (pD 7.9), 0.5 mM EDTA, 0.5 mM Mg-ADP-BeFx, 140 mM KCl, 0.5 mM $MgCl_2$. All the pH adjustments were done with DCl or NaOD. The nucleosome concentration used was 30 μM for the H4 ILV-labeled experiments and 40 μM for the H2A ILV experiments.

For the experiment involving SNF2h-nucleosome complex, SNF2h was buffer exchanged in the NMR buffer. Nucleosome and SNF2h were mixed in a 1:2 molar ratio to get two SNF2h molecules per nucleosome. The SNF2h concentration was saturating in the concentration regime used. For H4 ILV NMR experiments, the SNF2h concentration was ~60 μM and for the H2A ILV NMR experiments, the SNF2h concentration was 80 μM. This was done to ensure saturation of the binding sites because SNF2h is known to bind as a dimer to nucleosomes.

All the NMR spectra were acquired at 25°C on a Bruker 600 MHz spectrometer equipped with a cryoprobe. Recorded spectra were processed using the NMRPipe software (*63*) and displayed using SPARKY (*64*). In case of H4-ILV nucleosome, the assignments were transferred from published spectra of Drosophila nucleosome by inspection (*20*). The two sets of spectra were remarkably similar owing to complete sequence conservation between *Drosophila* and *Xenopus* histones H4 (fig. S1). A comparison of the chemical-shift positions across *Drosophila* and *Xenopus* histone H4 spectra suggested very small differences between the two, with the average Δδppm being 0.1 (fig. S2). The two spectra were acquired under different buffer conditions, and at different temperatures [45°C for *Drosophila* (*20*), 25°C for *Xenopus* in the present work]. These two factors—buffer and temperature—together can help explain minor differences seen between the two sets of spectra.

Native gel–based remodeling assays

The cross-linked nucleosome preparations have a higher amount of free DNA. Therefore, to make sure we rigorously compare cross-linked and uncross-linked nucleosomes under the same conditions, we add free Cy3 labeled DNA to the uncross-linked nucleosomes (WT) to make the free DNA concentrations the same for cross-linked and WT nucleosome reactions. Higher amounts of free DNA added reduce the remodeling rate of WT nucleosomes because of competition with the free DNA (fig. S8, C and D). In this context, ACF is more inhibited than SNF2h by comparable amounts of added DNA.

Remodeling assays were carried out on nucleosomal templates containing 60 bp of flanking DNA (601+60). Native gel–based remodeling assays with nucleosomes containing WT and mutant histones were carried out in the presence of 300 nM SNF2h and 30 nM nucleosomes as described (*65*). The final reaction buffer was 20 mM Tris (pH 7.5), 70 mM KCl, 5 mM $MgCl_2$, 0.02% NP-40, 2 mM ATP. The nucleosomes were labeled with Cy3 on the long end of DNA fragment for detection by fluorescence-based scanning. For experiments involving dCx nucleosomes and SNF2h (Fig. 2D), 6 nM of free DNA was added; in the case of remodeling experiments with sCx1 nucleosomes (Fig. 3, A and 3B), ~2 nM free DNA was added and with sCx2 nucleosomes, ~1.5 nM of free DNA was added.

The RSC experiment was done with 20 nM 601 30-30 centered nucleosomes and 50 nM RSC. The buffer used in remodeling reaction with RSC was 30 mM Tris (pH 7.5), 50 mM KCl, 1 mM $MgCl_2$, 4% glycerol, 0.02% NP-40, 20 μM ATP. To the WT sample, 15 nM free DNA was externally added to make the reaction comparable to that of dCx nucleosome remodeling. INO80 remodeling

reactions were performed with 30 nM nucleosomes and 60 nM enzyme under the following conditions: 25 mM Tris (pH 7.5), 25 mM HEPES (pH 7.5), 100 mM KCl, 10% glycerol, 2 mM $MgCl_2$, 2 mM DTT, 1 mM EDTA, 100 μM ATP. It should be noted that 2 mM DTT present in the buffer is not sufficient to reduce the disulfides to any detectable extent in dCx nucleosomes, even over time scales well beyond the time scale of this experiment. In addition, 4.5 nM DNA was added to the WT nucleosome sample to make the conditions comparable to those of the dCX sample. Remodeling was followed at different time points by allowing the reaction to proceed for the desired duration, followed by quenching the reaction with a stop solution containing excess free DNA and ADP. The samples corresponding to different time points were run on a 5.5% native polyacrylamide gel and visualized with a Typhoon scanner. The quantification of the gel images was done with ImageQuant software. All the other data analysis and fitting were performed with IgorPro.

For remodeling experiments using SNF2h and ACF, the fraction centered was calculated by dividing the signal intensity of centered nucleosome band by the total signal intensity of all nucleosomal species. In the case of the remodeling experiments involving RSC, the fraction of centered nucleosome (Fig. 4B, middle left panel) was calculated by dividing the signal intensity of centered nucleosome band by the total signal in the lane, which included free DNA. The fraction of off-centered nucleosomes (Fig. 4B, middle right panel) was calculated as the ratio of combined signal intensity of all the noncentered nucleosome bands to total signal in the lane; likewise, the fraction of free DNA was calculated as a ratio of signal intensity of the DNA band to that of total signal in the lane. The fraction of nucleosomes evicted at 2 min (Fig. 4B, lower right panel) was calculated as a ratio of DNA signal intensity at a given time (corrected for signal of DNA initially present at $t = 0$) to total starting nucleosome signal.

ATPase assays

The ATPase rate of SNF2h with WT and dCX nucleosomes was measured using the NADH (nicotinamide adenine dinucleotide, reduced) oxidation–coupled ATPase assay (*66*). The buffer for ATPase reaction contained 20 mM Tris (pH 7.5), 70 mM KCl, 5 mM $MgCl_2$, 2 mM ATP, 300 μM NADH, 2 mM phosphoenolpyruvate, pyruvate kinase (25 units/μl), lactate dehydrogenase (25 units/μl), 100 nM nucleosomes, 300 nM SNF2h. The reaction was monitored on a SpectraMax M5 plate reader (Molecular Devices).

SNF2h binding assay

For the binding assay, 20 nM of Cy3-labeled 601+20 nucleosome was incubated with varying concentrations of SNF2h, ranging from 0 to 600 nm in a buffer containing 20 mM Tris (pH 7.5), 0.5 mM Mg^{2+}-ADP-BeFx, and 0.5 mM free Mg^{2+} for ~40 min at room temperature. Products of the binding reaction were separated on a 3.5% native gel and analyzed by scanning for Cy3 fluorescence on a Typhoon scanner.

REFERENCES AND NOTES

1. L. Ho, G. R. Crabtree, Chromatin remodelling during development. *Nature* **463**, 474–484 (2010). doi: 10.1038/nature08911; pmid: 20110991
2. C. R. Clapier, B. R. Cairns, The biology of chromatin remodeling complexes. *Annu. Rev. Biochem.* **78**, 273–304 (2009). doi: 10.1146/annurev.biochem.77.062706.153223; pmid: 19355820
3. G. J. Narlikar, R. Sundaramoorthy, T. Owen-Hughes, Mechanisms and functions of ATP-dependent chromatin-remodeling enzymes. *Cell* **154**, 490–503 (2013). doi: 10.1016/j.cell.2013.07.011; pmid: 23911317
4. K. Luger, A. W. Mäder, R. K. Richmond, D. F. Sargent, T. J. Richmond, Crystal structure of the nucleosome core particle at 2.8 A resolution. *Nature* **389**, 251–260 (1997). doi: 10.1038/38444; pmid: 9305837
5. A. Saha, J. Wittmeyer, B. R. Cairns, Chromatin remodeling by RSC involves ATP-dependent DNA translocation. *Genes Dev.* **16**, 2120–2134 (2002). doi: 10.1101/gad.995002; pmid: 12183366
6. G. Lia *et al*., Direct observation of DNA distortion by the RSC complex. *Mol. Cell* **21**, 417–425 (2006). doi: 10.1016/j.molcel.2005.12.013; pmid: 16455496
7. I. Whitehouse, C. Stockdale, A. Flaus, M. D. Szczelkun, T. Owen-Hughes, Evidence for DNA translocation by the ISWI chromatin-remodeling enzyme. *Mol. Cell. Biol.* **23**, 1935–1945 (2003). doi: 10.1128/MCB.23.6.1935-1945.2003; pmid: 12612068
8. Y. Zhang *et al*., DNA translocation and loop formation mechanism of chromatin remodeling by SWI/SNF and RSC. *Mol. Cell* **24**, 559–568 (2006). doi: 10.1016/j.molcel.2006.10.025; pmid: 17188033
9. S. Deindl *et al*., ISWI remodelers slide nucleosomes with coordinated multi-base-pair entry steps and single-base-pair exit steps. *Cell* **152**, 442–452 (2013). doi: 10.1016/j.cell.2012.12.040; pmid: 23374341
10. H. Y. Fan, X. He, R. E. Kingston, G. J. Narlikar, Distinct strategies to make nucleosomal DNA accessible. *Mol. Cell* **11**, 1311–1322 (2003). doi: 10.1016/S1097-2765(03)00192-8; pmid: 12769854
11. G. J. Narlikar, H. Y. Fan, R. E. Kingston, Cooperation between complexes that regulate chromatin structure and transcription. *Cell* **108**, 475–487 (2002). doi: 10.1016/S0092-8674(02)00654-2; pmid: 11909519
12. G. Schnitzler, S. Sif, R. E. Kingston, Human SWI/SNF interconverts a nucleosome between its base state and a stable remodeled state. *Cell* **94**, 17–27 (1998). doi: 10.1016/S0092-8674(00)81217-9; pmid: 9674423
13. Y. Lorch, B. R. Cairns, M. Zhang, R. D. Kornberg, Activated RSC-nucleosome complex and persistently altered form of the nucleosome. *Cell* **94**, 29–34 (1998). doi: 10.1016/S0092-8674(00)81218-0; pmid: 9674424
14. J. Côté, C. L. Peterson, J. L. Workman, Perturbation of nucleosome core structure by the SWI/SNF complex persists after its detachment, enhancing subsequent transcription factor binding. *Proc. Natl. Acad. Sci. U.S.A.* **95**, 4947–4952 (1998). doi: 10.1073/pnas.95.9.4947; pmid: 9560208
15. C. Y. Zhou, S. L. Johnson, N. I. Gamarra, G. J. Narlikar, Mechanisms of ATP-Dependent Chromatin Remodeling Motors. *Annu. Rev. Biophys.* **45**, 153–181 (2016). doi: 10.1146/annurev-biophys-051013-022819; pmid: 27391925
16. M. Alilat, A. Sivolob, B. Révet, A. Prunell, Nucleosome dynamics. Protein and DNA contributions in the chiral transition of the tetrasome, the histone (H3-H4)2 tetramer-DNA particle. *J. Mol. Biol.* **291**, 815–841 (1999). doi: 10.1006/jmbi.1999.2988; pmid: 10452891
17. R. Rosenzweig, L. E. Kay, Bringing dynamic molecular machines into focus by methyl-TROSY NMR. *Annu. Rev. Biochem.* **83**, 291–315 (2014). doi: 10.1146/annurev-biochem-060713-035829; pmid: 24905784
18. R. Sprangers, A. Gribun, P. M. Hwang, W. A. Houry, L. E. Kay, Quantitative NMR spectroscopy of supramolecular complexes: Dynamic side pores in ClpP are important for product release. *Proc. Natl. Acad. Sci. U.S.A.* **102**, 16678–16683 (2005). doi: 10.1073/pnas.0507370102; pmid: 16263929
19. R. Sprangers, L. E. Kay, Quantitative dynamics and binding studies of the 20S proteasome by NMR. *Nature* **445**, 618–622 (2007). doi: 10.1038/nature05512; pmid: 17237764
20. H. Kato *et al*., Architecture of the high mobility group nucleosomal protein 2-nucleosome complex as revealed by methyl-based NMR. *Proc. Natl. Acad. Sci. U.S.A.* **108**, 12283–12288 (2011). doi: 10.1073/pnas.1105848108; pmid: 21730181
21. L. R. Racki *et al*., The chromatin remodeller ACF acts as a dimeric motor to space nucleosomes. *Nature* **462**, 1016–1021 (2009). doi: 10.1038/nature08621; pmid: 20033039
22. C. R. Clapier, G. Längst, D. F. Corona, P. B. Becker, K. P. Nightingale, Critical role for the histone H4 N terminus in nucleosome remodeling by ISWI. *Mol. Cell. Biol.* **21**, 875–883 (2001). doi: 10.1128/MCB.21.3.875-883.2001; pmid: 11154274
23. A. Hamiche, J. G. Kang, C. Dennis, H. Xiao, C. Wu, Histone tails modulate nucleosome mobility and regulate ATP-dependent nucleosome sliding by NURF. *Proc. Natl. Acad. Sci. U.S.A.* **98**, 14316–14321 (2001). doi: 10.1073/pnas.251421398; pmid: 11724935
24. C. R. Clapier, K. P. Nightingale, P. B. Becker, A critical epitope for substrate recognition by the nucleosome remodeling ATPase ISWI. *Nucleic Acids Res.* **30**, 649–655 (2002). doi: 10.1093/nar/30.3.649; pmid: 11809876
25. W. Dang, M. N. Kagalwala, B. Bartholomew, Regulation of ISW2 by concerted action of histone H4 tail and extranucleosomal DNA. *Mol. Cell. Biol.* **26**, 7388–7396 (2006). doi: 10.1128/MCB.01159-06; pmid: 17015471
26. L. R. Racki *et al*., The histone H4 tail regulates the conformation of the ATP-binding pocket in the SNF2h chromatin remodeling enzyme. *J. Mol. Biol.* **426**, 2034–2044 (2014). doi: 10.1016/j.jmb.2014.02.021; pmid: 24607692
27. V. Tugarinov, P. M. Hwang, J. E. Ollerenshaw, L. E. Kay, Cross-correlated relaxation enhanced 1H[bond]13C NMR spectroscopy of methyl groups in very high molecular weight proteins and protein complexes. *J. Am. Chem. Soc.* **125**, 10420–10428 (2003). doi: 10.1021/ja030153x; pmid: 12926967
28. A. Mittermaier, L. E. Kay, New tools provide new insights in NMR studies of protein dynamics. *Science* **312**, 224–228 (2006). doi: 10.1126/science.1124964; pmid: 16614210
29. D. J. Hamel, F. W. Dahlquist, The contact interface of a 120 kD CheA-CheW complex by methyl TROSY interaction spectroscopy. *J. Am. Chem. Soc.* **127**, 9676–9677 (2005). doi: 10.1021/ja052517m; pmid: 15998058
30. M. Schlosshauer, D. Baker, Realistic protein-protein association rates from a simple diffusional model neglecting long-range interactions, free energy barriers, and landscape ruggedness. *Protein Sci.* **13**, 1660–1669 (2004). doi: 10.1110/ps.03517304; pmid: 15133165
31. W. Dang, B. Bartholomew, Domain architecture of the catalytic subunit in the ISW2-nucleosome complex. *Mol. Cell. Biol.* **27**, 8306–8317 (2007). doi: 10.1128/MCB.01351-07; pmid: 17908792
32. M. Zofall, J. Persinger, S. R. Kassabov, B. Bartholomew, Chromatin remodeling by ISW2 and SWI/SNF requires DNA translocation inside the nucleosome. *Nat. Struct. Mol. Biol.* **13**, 339–346 (2006). doi: 10.1038/nsmb1071; pmid: 16518397
33. M. N. Kagalwala, B. J. Glaus, W. Dang, M. Zofall, B. Bartholomew, Topography of the ISW2-nucleosome complex: Insights into nucleosome spacing and chromatin remodeling. *EMBO J.* **23**, 2092–2104 (2004). doi: 10.1038/sj.emboj.7600220; pmid: 15131696
34. www.bmrb.wisc.edu.
35. W. Kruger *et al*., Amino acid substitutions in the structured domains of histones H3 and H4 partially relieve the requirement of the yeast SWI/SNF complex for transcription. *Genes Dev.* **9**, 2770–2779 (1995). doi: 10.1101/gad.9.22.2770; pmid: 7590252
36. U. M. Muthurajan *et al*., Crystal structures of histone Sin mutant nucleosomes reveal altered protein-DNA interactions. *EMBO J.* **23**, 260–271 (2004). doi: 10.1038/sj.emboj.7600046; pmid: 14739929
37. A. Flaus, C. Rencurel, H. Ferreira, N. Wiechens, T. Owen-Hughes, Sin mutations alter inherent nucleosome mobility. *EMBO J.* **23**, 343–353 (2004). doi: 10.1038/sj.emboj.7600047; pmid: 14726954
38. P. J. Horn, K. A. Crowley, L. M. Carruthers, J. C. Hansen, C. L. Peterson, The SIN domain of the histone octamer is essential for intramolecular folding of nucleosomal arrays. *Nat. Struct. Biol.* **9**, 167–171 (2002). pmid: 11836537
39. T. Tsukiyama, C. Wu, Purification and properties of an ATP-dependent nucleosome remodeling factor. *Cell* **83**, 1011–1020 (1995). doi: 10.1016/0092-8674(95)90216-3; pmid: 8521501
40. T. Ito, M. Bulger, M. J. Pazin, R. Kobayashi, J. T. Kadonaga, ACF, an ISWI-containing and ATP-utilizing chromatin assembly

and remodeling factor. *Cell* **90**, 145–155 (1997). doi: 10.1016/S0092-8674(00)80321-9; pmid: 9230310
41. J. D. Aalfs, G. J. Narlikar, R. E. Kingston, Functional differences between the human ATP-dependent nucleosome remodeling proteins BRG1 and SNF2H. *J. Biol. Chem.* **276**, 34270–34278 (2001). doi: 10.1074/jbc.M104163200; pmid: 11435432
42. D. F. V. Corona *et al*., ISWI is an ATP-dependent nucleosome remodeling factor. *Mol. Cell* **3**, 239–245 (1999). doi: 10.1016/S1097-2765(00)80314-7; pmid: 10078206
43. C. Horigome *et al*., SWR1 and INO80 chromatin remodelers contribute to DNA double-strand break perinuclear anchorage site choice. *Mol. Cell* **55**, 626–639 (2014). doi: 10.1016/j.molcel.2014.06.027; pmid: 25066231
44. X. Shen, G. Mizuguchi, A. Hamiche, C. Wu, A chromatin remodelling complex involved in transcription and DNA processing. *Nature* **406**, 541–544 (2000). doi: 10.1038/35020123; pmid: 10952318
45. M. Udugama, A. Sabri, B. Bartholomew, The INO80 ATP-dependent chromatin remodeling complex is a nucleosome spacing factor. *Mol. Cell. Biol.* **31**, 662–673 (2011). doi: 10.1128/MCB.01035-10; pmid: 21135121
46. A. Tosi *et al*., Structure and subunit topology of the INO80 chromatin remodeler and its nucleosome complex. *Cell* **154**, 1207–1219 (2013). doi: 10.1016/j.cell.2013.08.016; pmid: 24034245
47. M. Bruno *et al*., Histone H2A/H2B dimer exchange by ATP-dependent chromatin remodeling activities. *Mol. Cell* **12**, 1599–1606 (2003). doi: 10.1016/S1097-2765(03)00499-4; pmid: 14690611
48. B. T. Harada *et al*., Stepwise nucleosome translocation by RSC remodeling complexes. *eLife* **5**, e10051 (2016). doi: 10.7554/eLife.10051; pmid: 26895087
49. V. K. Gangaraju, P. Prasad, A. Srour, M. N. Kagalwala, B. Bartholomew, Conformational changes associated with template commitment in ATP-dependent chromatin remodeling by ISW2. *Mol. Cell* **35**, 58–69 (2009). doi: 10.1016/j.molcel.2009.05.013; pmid: 19595716
50. J. D. Leonard, G. J. Narlikar, A nucleotide-driven switch regulates flanking DNA length sensing by a dimeric chromatin remodeler. *Mol. Cell* **57**, 850–859 (2015). doi: 10.1016/j.molcel.2015.01.008; pmid: 25684208
51. C. R. Clapier *et al*., Regulation of DNA Translocation Efficiency within the Chromatin Remodeler RSC/Sth1 Potentiates Nucleosome Sliding and Ejection. *Mol. Cell* **62**, 453–461 (2016). doi: 10.1016/j.molcel.2016.03.032; pmid: 27153540
52. J. R. Guyon, G. J. Narlikar, E. K. Sullivan, R. E. Kingston, Stability of a human SWI-SNF remodeled nucleosomal array. *Mol. Cell. Biol.* **21**, 1132–1144 (2001). doi: 10.1128/MCB.21.4.1132-1144.2001; pmid: 11158300
53. A. N. Imbalzano, G. R. Schnitzler, R. E. Kingston, Nucleosome disruption by human SWI/SNF is maintained in the absence of continued ATP hydrolysis. *J. Biol. Chem.* **271**, 20726–20733 (1996). doi: 10.1074/jbc.271.34.20726; pmid: 8702824
54. L. A. Boyer, X. Shao, R. H. Ebright, C. L. Peterson, Roles of the histone H2A-H2B dimers and the (H3-H4)(2) tetramer in nucleosome remodeling by the SWI-SNF complex. *J. Biol. Chem.* **275**, 11545–11552 (2000). doi: 10.1074/jbc.275.16.11545; pmid: 10766768
55. D. P. Bazett-Jones, J. Côté, C. C. Landel, C. L. Peterson, J. L. Workman, The SWI/SNF complex creates loop domains in DNA and polynucleosome arrays and can disrupt DNA-histone contacts within these domains. *Mol. Cell. Biol.* **19**, 1470–1478 (1999). doi: 10.1128/MCB.19.2.1470; pmid: 9891080
56. A. J. Andrews, K. Luger, Nucleosome structure(s) and stability: Variations on a theme. *Annu. Rev. Biophys.* **40**, 99–117 (2011). doi: 10.1146/annurev-biophys-042910-155329; pmid: 21332355
57. C. P. Prior, C. R. Cantor, E. M. Johnson, V. C. Littau, V. G. Allfrey, Reversible changes in nucleosome structure and histone H3 accessibility in transcriptionally active and inactive states of rDNA chromatin. *Cell* **34**, 1033–1042 (1983). doi: 10.1016/0092-8674(83)90561-5; pmid: 6313204
58. J. Fei *et al*., The prenucleosome, a stable conformational isomer of the nucleosome. *Genes Dev.* **29**, 2563–2575 (2015). pmid: 26680301
59. M. S. Cosgrove, J. D. Boeke, C. Wolberger, Regulated nucleosome mobility and the histone code. *Nat. Struct. Mol. Biol.* **11**, 1037–1043 (2004). doi: 10.1038/nsmb851; pmid: 15523479
60. K. S. Zaret, J. S. Carroll, Pioneer transcription factors: Establishing competence for gene expression. *Genes Dev.* **25**, 2227–2241 (2011). doi: 10.1101/gad.176826.111; pmid: 22056668
61. P. N. Dyer *et al*., Reconstitution of nucleosome core particles from recombinant histones and DNA. *Methods Enzymol.* **375**, 23–44 (2004). doi: 10.1016/S0076-6879(03)75002-2; pmid: 14870657
62. V. Tugarinov, V. Kanelis, L. E. Kay, Isotope labeling strategies for the study of high-molecular-weight proteins by solution NMR spectroscopy. *Nat. Protoc.* **1**, 749–754 (2006). doi: 10.1038/nprot.2006.101; pmid: 17406304
63. F. Delaglio *et al*., NMRPipe: A multidimensional spectral processing system based on UNIX pipes. *J. Biomol. NMR* **6**, 277–293 (1995). doi: 10.1007/BF00197809; pmid: 8520220
64. T. D. Goddard, D. G. Kneller, University of California San Francisco, "SPARKY 3" (1996).
65. J. G. Yang, T. S. Madrid, E. Sevastopoulos, G. J. Narlikar, The chromatin-remodeling enzyme ACF is an ATP-dependent DNA length sensor that regulates nucleosome spacing. *Nat. Struct. Mol. Biol.* **13**, 1078–1083 (2006). doi: 10.1038/nsmb1170; pmid: 17099699
66. J. E. Lindsley, Use of a real-time, coupled assay to measure the ATPase activity of DNA topoisomerase II. *Methods Mol. Biol.* **95**, 57–64 (2001). pmid: 11089219
67. C. A. Davey, D. F. Sargent, K. Luger, A. W. Maeder, T. J. Richmond, Solvent mediated interactions in the structure of the nucleosome core particle at 1.9 a resolution. *J. Mol. Biol.* **319**, 1097–1113 (2002). doi: 10.1016/S0022-2836(02)00386-8; pmid: 12079350
68. L. Cavallo, J. Kleinjung, F. Fraternali, POPS: A fast algorithm for solvent accessible surface areas at atomic and residue level. *Nucleic Acids Res.* **31**, 3364–3366 (2003). doi: 10.1093/nar/gkg601; pmid: 12824328

ACKNOWLEDGMENTS

We thank J. Tretyakova for her tireless effort in preparing histones, C. Zhou for generously providing yeast INO80 complex, N. Gamarra for generously providing ACF, and J. Pelton and the QB3 NMR Facility at the University of California Berkeley for help with collecting NMR data. We thank T. Richmond for the plasmid containing repeats of the 601+20 sequence. We thank C. Zhou and J. Leonard for helpful comments on the manuscript and members of the Narlikar laboratory for stimulating discussions. This work was supported by a grant from the Program for Breakthrough Biomedical Research at UCSF to G.J.N. and J.D.G., a grant from the NIH to G.J.N. (R01GM073767), and a Postdoctoral Fellowship from the Human Frontiers Science Program to K.K.S. K.K.S. and G.J.N. identified and developed the core mechanistic questions, and J.D.G. identified NMR as a powerful approach for addressing this question. K.K.S. performed all the experiments, J.D.G. guided the NMR experiments and helped K.K.S. and G.J.N. interpret the NMR data. K.K.S., J.D.G., and G.J.N. wrote the manuscript. G.J.N. oversaw the project. Supplementary figures and supplementary figure legends are described in the supplementary materials.

SUPPLEMENTARY MATERIALS

www.sciencemag.org/content/355/6322/eaaa3761/suppl/DC1
Figs. S1 to S8

13 July 2016; resubmitted 26 September 2016
Accepted 5 December 2016
10.1126/science.aaa3761

Distortion of histone octamer core promotes nucleosome mobilization by a chromatin remodeler

Kalyan K. Sinha, John D. Gross and Geeta J. Narlikar

Science **355** (6322), eaaa3761.
DOI: 10.1126/science.aaa3761

Deformation powers the nucleosome slide

In eukaryotes, DNA is packed onto nucleosomes. For transcription factors and other proteins to gain access to DNA, nucleosomes must be moved out of the way, or "remodeled"—but not disassembled. Nucleosomes are composed of histone protein octamers, the cores of which have generally been considered to be fairly rigid. Sinha *et al.* used nuclear magnetic resonance and protein cross-linking to show that one of the enzyme complexes that remodel nucleosomes, SNF2h, is able to distort the histone octamer (see the Perspective by Flaus and Owen-Hughes). Nucleosome deformation was important for this remodeler to be able to slide nucleosomes out of the way.

Science, this issue p. 10.1126/science.aaa3761 ; see also p. 245